ELSEVIER

Check for updates

A myeloperoxidase-responsive and biodegradable luminescent material for real-time imaging of inflammatory diseases

Jiawei Guo [1,†], Hui Tao [1,†], Yin Dou [1,†], Lanlan Li [1], Xiaoqiu Xu [1], Qixiong Zhang [1], Juan Cheng [1], Songling Han [1,2], Jun Huang [3], Xiaodong Li [2,*], Xiaohui Li [1], Jianxiang Zhang [1,*]

[1] Department of Pharmaceutics, College of Pharmacy, Third Military Medical University, Chongqing 400038, China
[2] Affiliated Stomatology Hospital, School of Medicine, Zhejiang University, Hangzhou 310068, China
[3] Institute for Molecular Engineering, University of Chicago, Chicago, IL 60637, USA

We report the synthesis and characterization of a myeloperoxidase (MPO)-responsive, biodegradable, and luminescent material derived from functionalized cyclodextrin. The nanoparticle based on this functional material shows notably high and sustainable luminescent signals upon triggering by inflammatory conditions with abnormally elevated reactive oxygen species and MPO. Activated neutrophils during inflammatory responses can be selectively imaged using this nanoprobe, with luminescent signals positively correlated to neutrophil counts. This nanoprobe enables *in vivo* precise quantification and tracking of the number and dynamics of neutrophils in both superficial and deep tissues in various mouse models of inflammatory diseases, including peritonitis, paw edema, colitis, and acute lung injury. *In vitro* and *in vivo* evaluations also demonstrate the safety and biocompatibility of this newly engineered material in its native and nanoparticle forms.

Introduction

Inflammation has been implicated in the pathogenesis of many diseases including arthritis, Alzheimer's disease, cancer, and cardiovascular disease [1–3]. It is also a key feature of metabolic disorders such as obesity and diabetes [4]. As the most abundant leukocytes in the circulation, neutrophils play an important role in acute inflammatory responses by exerting their multiple functions [5–8]. Additionally, neutrophils are initiators of chronic inflammatory disorders, such as chronic obstructive pulmonary disease [9], arthritis [10], inflammatory bowel disease [11], and atherosclerosis [12]. Therefore, rapid detection, reliable tracking, and precise quantification of neutrophils under different conditions can address unmet demands for understanding, diagnosis, and therapy of inflammatory diseases. Traditionally, histological or immunohistochemical methods, scintigraphy, and flow cytometry have been utilized for either qualitative or quantitative detection of neutrophils. However, these techniques cannot provide anatomical information with desirable spatiotemporal resolutions in physiological environments. A common problem of those existing cell-labeling methods is that they are toxic to neutrophils. Furthermore, they are time-consuming and labor-intensive in sampling of tissues and cells. The sampling procedures often require animal sacrifice, eliminating the possibility to obtain dynamic information of neutrophil trafficking, proliferation, and death.

As a noninvasive, rapid, straightforward, and versatile approach, luminescence imaging enables direct observation of *in vitro* activation of inflammatory cells, longitudinal examination of neutrophil recruitment in the development of inflammation, and assessment of therapeutic responses to various treatments [13–16]. Small molecular luminescent probes, such as luminol and its analogs, are frequently used for *in vivo* detection of inflammation-associated diseases [17–20], via luminescence imaging of myeloperoxidase (MPO) activities in the presence of reactive molecular species, based on the abundant expression of MPO in neutrophils [21]. Unfortunately, these

* Corresponding authors.
E-mail addresses: Li, X. (cisarli@zju.edu.cn), Zhang, J. (jxzhang1980@gmail.com), (jxzhang@tmmu.edu.cn).
† These authors contributed equally to this work.

1369-7021/© 2017 Elsevier Ltd. All rights reserved. https://doi.org/10.1016/j.mattod.2017.09.003

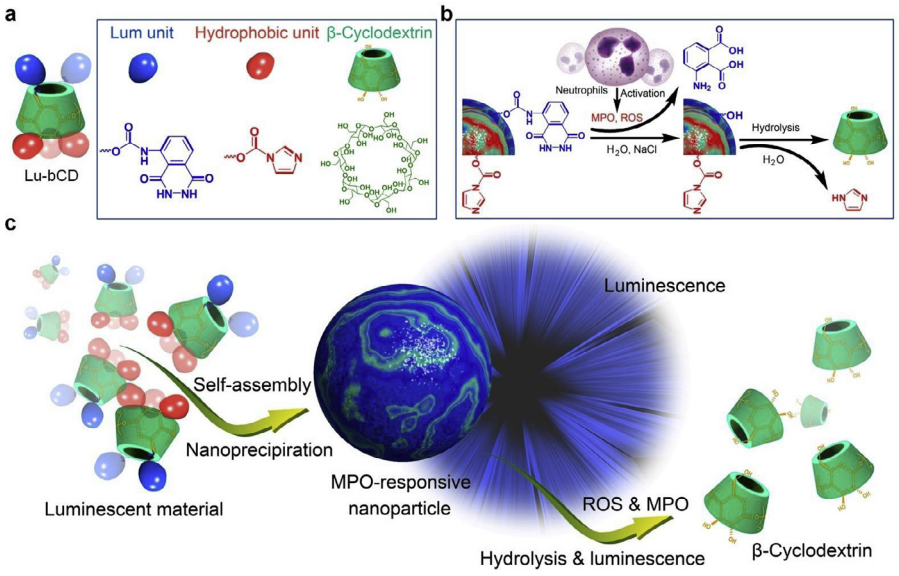

FIGURE 1

Design of a myeloperoxidase (MPO)-responsive, biodegradable, and luminescent material and nanoparticle. (a) Schematic of the structure and composition of the luminescent material derived from luminol (Lum)-conjugated b-cyclodextrin (Lu-bCD). (b) Responsive hydrolysis mechanism of the luminescent material. (c) Engineering of a MPO-responsive luminescent nanoparticle based on the functionalized cyclodextrin material.

small molecular agents are temporally limited due to the rapid decay of luminescent signals as a result of instant absorption and quick excretion [22]. Poor spatial resolution has also been observed for these probes, particularly for deep tissues, resulting from nonspecific distribution as well as tissue absorption and dissemination upon systemic administration [18]. To circumvent these issues, different nanoprobes have been developed recently based on conjugated polymers, inorganic materials, and metal–organic frameworks for *in vitro* and *in vivo* studies [23–31]. However, biodegradability and biocompatibility are currently the major limitation of *in vivo* applications of these luminescent nanomaterials. More importantly, their feasibility and quality of imaging inflammatory diseases remain to be demonstrated.

Herein we report a new luminescent material that is able to address above challenges. This functional material is derived from luminol-conjugated cyclodextrin, a molecule responsive to inflammation characterized by overproduction of reactive oxygen species (ROS) and MPO (Fig. 1). The nanoparticle (NP) based on this biodegradable luminescent material showed notably high and sustainable luminescence, compared with luminol itself in both *in vitro* cell culture and *in vivo* murine models of inflammatory diseases. Also, this luminescent nanoprobe efficiently illuminated deep tissue inflammation in an acute lung injury mouse model. Luminescent signals were well-correlated with neutrophil counts, in a large linear dynamic range, enabling *in vivo* precise quantification of neutrophil dynamics in inflammatory diseases or disorders.

Results and discussion

Synthesis of a MPO-responsive material and fabrication of a luminescent nanoparticle

The MPO-responsive luminescent material was synthesized by chemical modification of b-cyclodextrin (b-CD), a cyclic oligosaccharide with good *in vivo* safety [32]. This was achieved by activation of b-CD via 1,1′-carbonyldiimidazole (CDI), followed by conjugation of luminol (Lum) units on b-CD (Fig. S1a). While the covalently linked Lum units are relatively hydrophilic, the remained imidazole moieties are hydrophobic components, thereby giving rise to an amphiphilic material. Characterization by Fourier transform infrared (FT-IR) as well as ^{1}H and ^{13}C NMR spectrometry confirmed successful conjugation of Lum units in b-CD molecules (Fig. S2a–c). Thus obtained material Lu-bCD displayed similar UV–Visible absorption and fluorescence emission spectra as compared to those of free luminol (Fig. S2d-e). Measurement by matrix-assisted laser desorption/ionization time-of-flight mass spectrometry also affirmed the synthesis of Lu-bCD (Fig. S2f). Calculation based on the ^{1}H NMR spectrum and UV–Visible absorbance suggested about 1 Lum and 3 imidazole units were covalently linked to each b-CD molecule.

The NP based on the luminescent material Lu-bCD was produced by a nanoprecipitation/self-assembly method, leading to spherical Lu-bCD NP as observed by transmission electron microscopy (TEM) (Fig. 2a). Measurement of Lu-bCD NP from different batches by dynamic light scattering revealed mean diameter of 228 þ 19 nm ($n = 15$), with polydispersity of 0.11 þ 0.04 ($n = 15$). A representative size distribution profile is illustrated in the right panel of Fig. 2a. The relative small size observed in the TEM image might be due to dried particles under TEM conditions, while particles were swollen to a certain degree in aqueous solution. In the existence of H_2O_2, Lu-bCD NP could be slowly hydrolyzed (Fig. S3a), while hydrolysis was considerably accelerated upon incubation with ClO^- (Fig. S3b). This indicated that hydrolysis of Lu-bCD NP is more sensitive to ClO^-. Analysis by ^{1}H NMR and mass spectrometry suggested that Lu-bCD may be hydrolyzed to its parent compound b-CD (Figs. S3c-d and S1b).

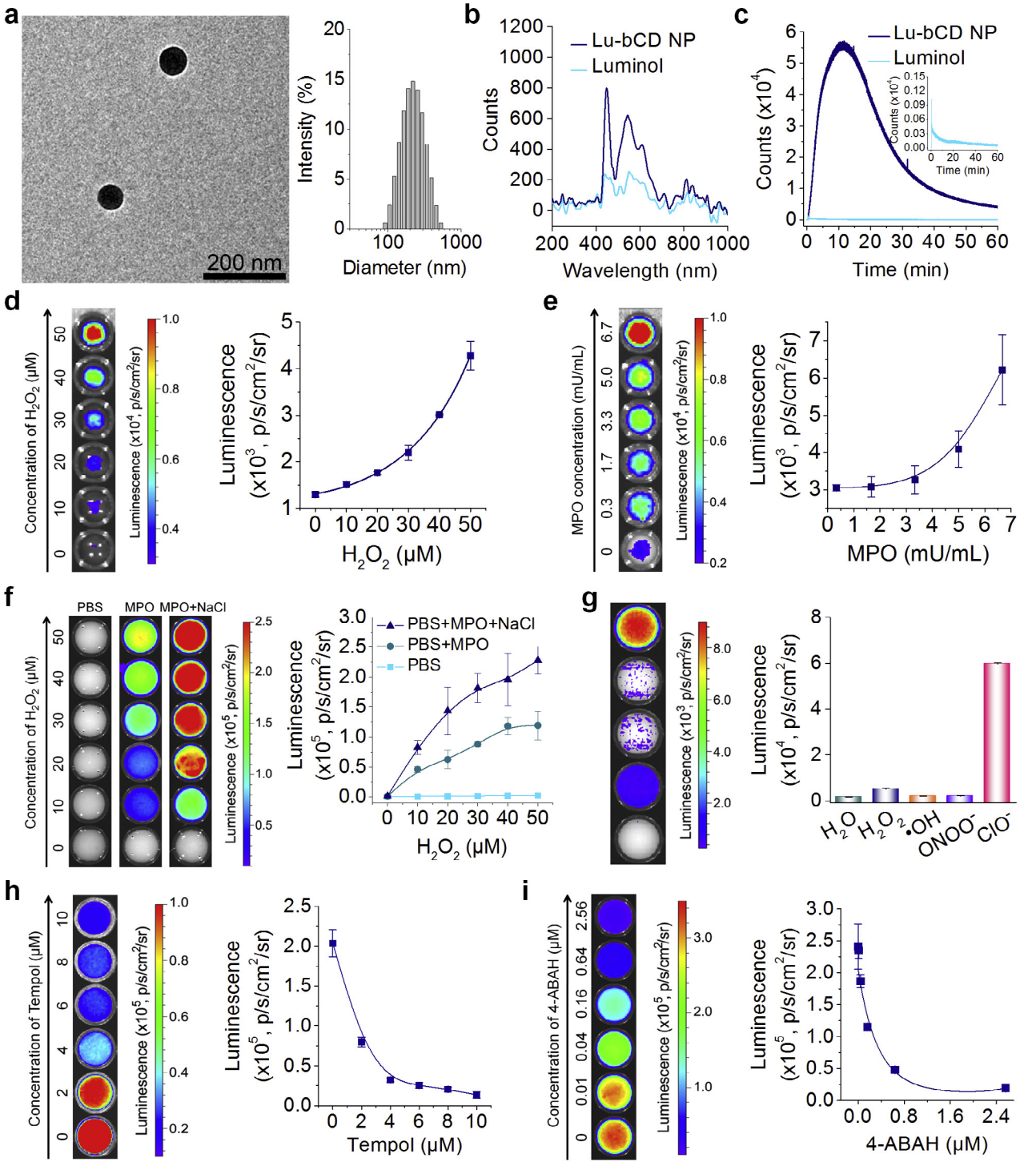

FIGURE 2

Characterization of the MPO-responsive luminescent nanoparticle. (a) TEM image and size distribution profile of Lu-bCD NP. (b and c) Luminescent spectra (b) and time dependent luminescent intensity (c) of luminol and Lu-bCD NP in the presence of H_2O_2 at 0.5 or 5 mM, respectively. In both cases, Lu-bCD NP and free luminol with the same content of Lum were used. (d and e) The effect of H_2O_2 (d) or MPO (e) levels on luminescence of Lu-bCD NP. In both cases, the left panel shows *ex vivo* luminescent images, while the right panel indicates quantitative analysis. (f) Enhanced luminescence of Lu-bCD NP by MPO and Cl^-. The left panel shows typical *ex vivo* images, while the right panel illustrates quantitative results. (g) The influence of ROS types on luminescence of Lu-bCD NP. (h and i) Typical luminescent images (left) and quantitative results (right) illustrating attenuation of Lu-bCD NP luminescence by a ROS scavenger Tempol (h) a MPO inhibitor 4-ABAH (i). Error bars, mean þ s.d. ($n = 3$).

Then we examined luminescent properties of Lu-bCD NP. Analyses by a fiber optic spectrometer showed that, at the same concentration of Lum, Lu-bCD NP displayed notably higher luminescent signals than free luminol at 1 mM H_2O_2 (Fig. 2b). Furthermore, Lu-bCD NP exhibited sustainably higher time-lapse luminescent intensities during the examined time period

of 1 h, as compared to luminol with the same dose of Lum (Fig. 2c). This sustainable and enhanced luminescence of Lu-bCD NP was also detected by imaging via an IVIS Spectrum system (Fig. S4a). Upon incubation with both low and high levels of H_2O_2, luminescent signals of Lu-bCD NP were increased as a function of the H_2O_2 level (Figs. 2d and S4b). In addition, luminescence was linearly increased with the Lu-bCD NP concentration (Fig. S4c). Also, we found enhanced luminescent intensity as the MPO level was increased (Fig. 2e). Independent of varied doses of H_2O_2, the presence of MPO remarkably potentiated luminescence of Lu-bCD NP, with additional strengthening by Cl^- (Fig. 2f), which may be due to the generation of a strong oxidizing anion ClO^- via the MPO–H_2O_2–Cl^- system [33]. In line with this, the luminescent signal of Lu-bCD NP was selectively enhanced by ClO^- (Fig. 2g). Notably, luminescence of Lu-bCD NP was significantly attenuated by eliminating ROS or inhibiting MPO activity using a ROS scavenger Tempol or a MPO inhibitor 4-ABAH, respectively (Fig. 2h and i). Collectively, these findings demonstrated that the MPO-responsive luminescent NP can be successfully developed using the material derived from Lum-functionalized b-CD. More importantly, luminescent signals were notably amplified by the nanoprobe as compared to free luminol. This enhanced luminescent strength and efficiency by the assembled NP should be attributed to increased peripheral presentation of Lum on the NP surface, which may increase efficiency of the reaction between Lum and oxidative species, resulting from increased encounter probability.

In vitro luminescence imaging of neutrophils

To examine whether our newly developed luminescent nanoprobe can be used to detect activated neutrophils that excrete both MPO and ROS, *in vitro* cell culture tests were conducted using neutrophils isolated from the peritoneal cavity of mice induced by intraperitoneal (*i.p.*) injection of thioglycollate (Fig. 3a). Fluorescence microscopy after staining with a fluorescent probe 2′,7′-dichlorofluorescin diacetate (DCFH-DA) revealed the generation of ROS after stimulation of neutrophils by phorbol 12-myristate 13-acetate (PMA) (Fig. 3b). Consistently, we observed significant luminescence in PMA-stimulated neutrophils using Lu-bCD NP (Fig. 3c). By contrast, only negligible luminescent signals appeared in the non-stimulated control. Consistent with the luminescence profile in the presence of H_2O_2, Lu-bCD NP showed sustained and strong signals for activated neutrophils (Fig. 3d and e), while free luminol displayed a rapidly decayed curve. Importantly, no significant luminescent signals were detected for PMA-stimulated RAW264.7 murine macrophages (Fig. 3f), although the production of ROS was found (Fig. 3g). The selectivity of Lu-bCD NP luminescence to activated neutrophils should be associated with the generation of both ROS and MPO, in line with the finding that luminescence of Lu-bCD NP may be intensified by MPO and MPO/Cl^-. Finally, we found that the luminescent signals in the cultured neutrophil system were positively associated with the number of neutrophils and the dose of Lu-bCD NP (Fig. 3h and i). Accordingly, our neutrophil culture experiments demonstrated that Lu-bCD NP can serve as an efficient luminescent nanoprobe for selective imaging of activated neutrophils *in vitro*.

In vivo luminescence imaging of acute inflammation in mice

Subsequently, we performed *in vivo* studies to test the bioluminescence imaging potential of Lu-bCD NP in acute inflammation. First, mouse models of peritonitis were induced by *i.p.* injection with different stimulators including lipopolysaccharide (LPS), thioglycollate, and zymosan. Flow cytometry analyses revealed the number of neutrophils in peritoneal exudates was dependent on the type of stimulators (Fig. 4a). Concomitantly, we found increased production of MPO and ROS as well as inflammatory cytokines (TNF-a and IL-1b) in the cell-free lavage fluid (Figs. 4b and S5). After *i.p.* administration of Lu-bCD NP, *in vivo* imaging showed significant luminescent signals in mice, with a clear dependence on the stimulators (Fig. 4c). Of note, a good correlation was found between the number of neutrophils and the luminescent intensity (Fig. 4d). Additionally, luminescent signals were remarkably attenuated by either Tempol or 4-ABAH (Fig. 4e), well consistent with *in vitro* results (Fig. 2h and i). Also, Lu-bCD NP displayed sustained luminescence after only a single *i.p.* administration, while signals of free luminol at the same dose of Lum decayed exponentially (Fig. 4f). After *i.p.* injection of zymosan, gradually enhanced luminescent intensities were detected at 2, 4, and 6 h by Lu-bCD NP administered at the corresponding time points (Fig. 4g), which is consistent with the increased number of neutrophils in peritoneal exudates (Fig. 4h). Moreover, a good correlation was found between the luminescent signal and the neutrophil count (Fig. 4i). These experiments showed that the progression of peritonitis can be detected by luminescence imaging with Lu-bCD NP.

In another acute inflammation model of paw edema induced by intradermal (*i.d.*) injection of carrageen, which is also related to the infiltration of neutrophils [34], local administration of Lu-bCD NP showed longer and brighter luminescent signals compared to the same dose of free luminol (Fig. S6a). Comparatively, an exponential decay of luminescence was observed for luminol (Fig. S6b). After treatment with an anti-inflammatory drug dexamethasone (DEX), the luminescent intensity of Lu-bCD NP significantly decreased (Fig. S6c-d). This suggested that Lu-bCD NP luminescence is closely related to the degree of inflammation. We also examined the luminescence of Lu-bCD NP in mice with dextran sodium sulfate (DSS)-induced ulcerative colitis, which is characterized by excessive recruitment and accumulation of activated neutrophils in the colon as well as overproduction of MPO and ROS [11]. After administration of Lu-bCD NP by enema, significant luminescence was detected in mice with colitis (Fig. S7a-b). This is in accordance with the significant increase in MPO and ROS levels (Fig. S7c-d). By contrast, imaging with free luminol enema at the same dose of Lum failed to show significant difference between the normal and colitis animals (Fig. S7e). This might be due to the indiscriminate distribution and rapid absorption of small molecules, while NPs are able to specifically accumulate in the inflamed colon [35].

Taken together, Lu-bCD NP showed strong and long-lasting *in vivo* luminescence in the microenvironment of acute inflammation, clearly distinct from the weak and decaying signals of small molecular probes, therefore providing significant advantages for future basic research and clinical applications. These experiments demonstrated that Lu-bCD NP is an effective

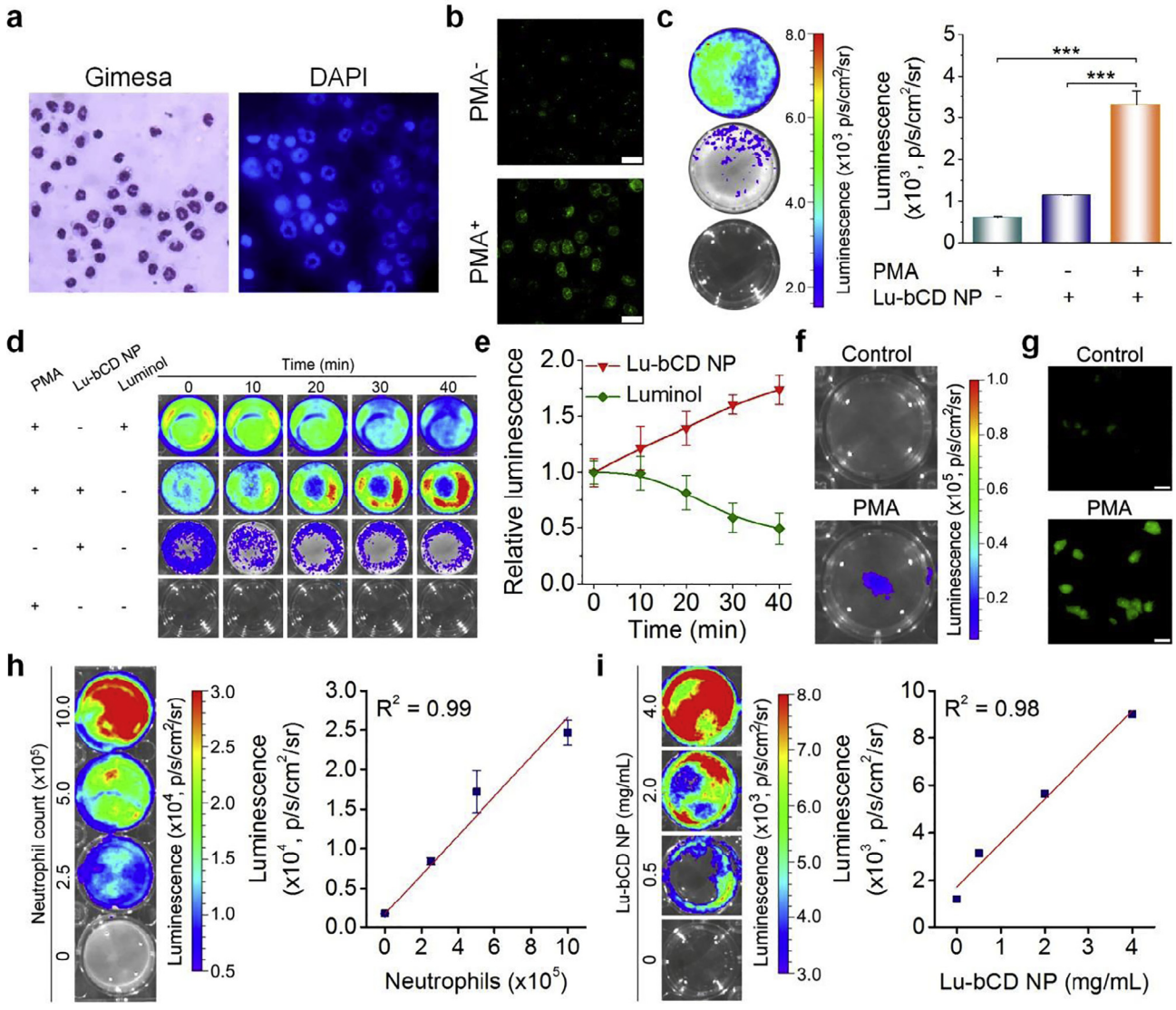

FIGURE 3

In vitro luminescence of Lu-bCD NP in neutrophils. (a) Optical microscopy images of Gimesa or DAPI stained neutrophils isolated from the peritoneal cavity of mice. (b) Fluorescence images illustrate the presence of ROS in PMA-stimulated neutrophils (PMA^+) stained by DCFH-DA. Scale bars, 20 lm. (c) Luminescent images (left) and quantitative histograms (right) of PMA-activated neutrophils after incubation with Lu-bCD NP. (d and e) Luminescence images (d) and quantitative analysis (e) of neutrophils treated with luminol or Lu-bCD NP. Cells were stimulated with 0.1 lg PMA for 1 h, followed by incubation with luminol or Lu-bCD NP at the same dose of Lum and imaging at different time points. (f) Luminescence images of control or PMA-stimulated RAW264.7 macrophages after incubation with Lu-bCD NP. Cells were incubated with PBS (control) or Lu-bCD NP, and simultaneously stimulated with 0.1 lg PMA for 2 h. (g) Fluorescence images of DCFH-DA stained control or PMA-stimulated RAW264.7 macrophages. Scale bars, 50 lm. (h and i) Effects of the neutrophil count (h) and Lu-bCD NP dose (i) on luminescent intensities. Left panels, luminescent images; right panels, quantitative data. To study the neutrophil count effect, neutrophils were stimulated with 100 ng/mL of PMA for 1 h. Imaging was then performed immediately after 3 mg/mL of Lu-bCD NP was added. For the experiment in (i), 5×10^5 neutrophils were used. Error bars, mean þ s.d. ($n = 3$); $^{***}P < 0.001$.

luminescent nanoprobe for the detection of acute inflammation by imaging neutrophil dynamics *in vivo*.

Luminescence imaging of acute lung injury in mice

To expand the applications of Lu-bCD NP for luminescence imaging of neutrophils in other diseases, we established a mouse model of acute lung injury (ALI) that is histopathologically characterized by neutrophilic alveolitis, with the most severe manifestation of acute respiratory distress syndrome [36]. ALI in mice was induced by intratracheal (*i.t.*) inoculation of LPS. After 6 h LPS exposure, both pulmonary tissues and bronchoalveolar lavage of ALI mice showed remarkably high levels of MPO and ROS as well as high expression of inflammatory cytokines TNF-a and IL-1b (Fig. S8a-b). The neutrophil counts in pulmonary tissues and bronchoalveolar lavage were also significantly increased (Figs. 5a and S8c). Hematoxylin and eosin (H&E) stained pathological sections showed the patchy nature of injury, inflammatory infiltration, and vascular congestion for the ALI mice (Fig. 5b). We then compared the luminescence imaging between free luminol and Lu-bCD NP in ALI mice. Notably, *i.v.*

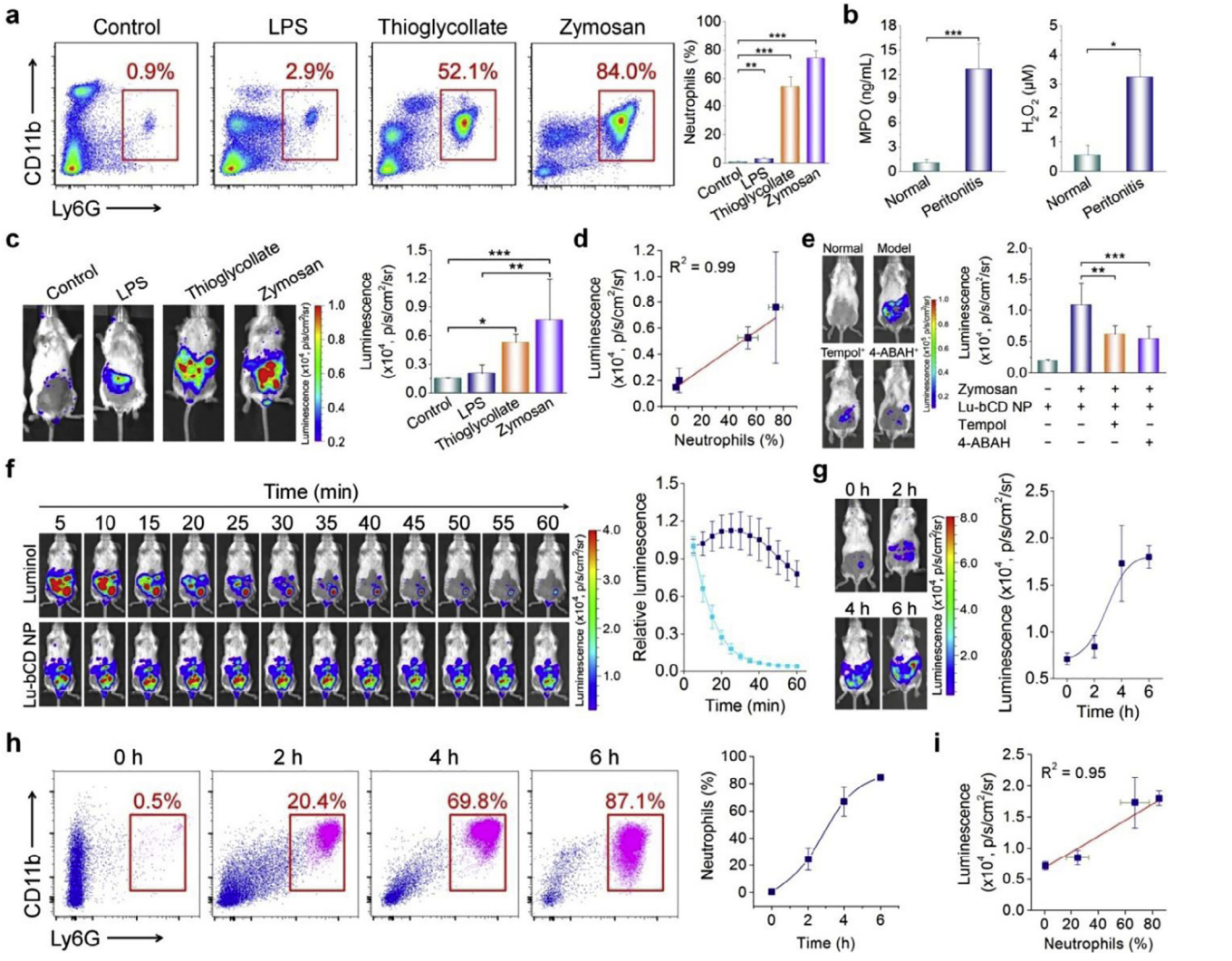

FIGURE 4

Luminescence imaging of peritonitis using Lu-bCD NP. (a) Quantification of neutrophils in peritoneal lavage of mice induced by intraperitoneal (*i.p.*) injection of different stimulators. The left panel shows representative flow cytometric profiles, while the right panel indicates the quantitative data. (b) The levels of MPO and H_2O_2 in cell-free peritoneal lavage of mice with peritonitis induced by *i.p.* injection of zymosan. (c) Typical *in vivo* images (left) and quantitative analysis (right) illustrating luminescence of mice with peritonitis induced by different stimulators. (d) Correlation between the neutrophil count and luminescent intensity. (e) Attenuation of Lu-bCD NP luminescence by a ROS scavenger Tempol or a MPO inhibitor 4-ABAH. The left and right panels separately show representative *in vivo* images and quantitative data. (f) Time dependent changes of luminescent signals in mice with peritonitis induced by *i.p.* zymosan. A single dose of either luminol or Lu-bCD NP at the same dose of the Lum unit was administered by *i.p.* injection at 6 h after stimulation with zymosan, and then, *in vivo* imaging was performed at different time points. Left panel, luminescence images; right panel, quantitative data. (g) Representative images (left) and quantitative results (right) illustrating *in vivo* luminescent intensities at various time points after *i.p.* injection of zymosan. Immediately after *i.p.* injection of Lu-bCD NP at 20 mg per mouse at the examined time points, *in vivo* imaging was conducted. (h) Quantification of neutrophils at various time points after *i.p.* injection of zymosan. (i) Linear correlation between the neutrophil count and luminescent signals. Error bars, mean þ s.d. ($n = 6$, a–b, h; $n = 4$, c, e–g); $^{*}P < 0.05$, $^{**}P < 0.01$, $^{***}P < 0.001$.

administration of Lu-bCD NP in normal mice showed negligible luminescent intensities (Fig. 5c), which might be important for accurate diagnosis of ALI. For luminol, quantitative analysis showed no differences before and after intravenous (*i.v.*) injection (Fig. 5d). By contrast, Lu-bCD NP offered much better luminescent signals. Consistently, we demonstrated pulmonary accumulation of Lu-bCD NP, labeled with a near infrared fluorescent dye Cy7.5 (Figs. S9 and 5e). Therefore, the luminescent nanoprobe Lu-bCD NP can be utilized to detect ALI by targeting the neutrophils of the injured sites.

We further tracked the dynamic progression of ALI in mice by Lu-bCD NP. After *i.t.* inoculation of LPS, luminescent signals were observed at the pulmonary sites of mice at different time points (the left panel, Fig. 5f), following a parabolic profile peaked at 6 h (the right panel, Fig. 5f). Consistently, flow cytometric analysis showed a similar trend of neutrophil dynamics in the lung tissues (Fig. 5g and h). Also, the levels of MPO and H_2O_2 changed accordingly at the examined time points (Fig. 5i). Again, the luminescent signals were well-correlated with the counts of neutrophils and the levels of MPO and ROS during ALI process (Fig. 5j). Together, these results substantiated that Lu-bCD NP is an efficient luminescent nanoprobe to detect the progression and development of ALI.

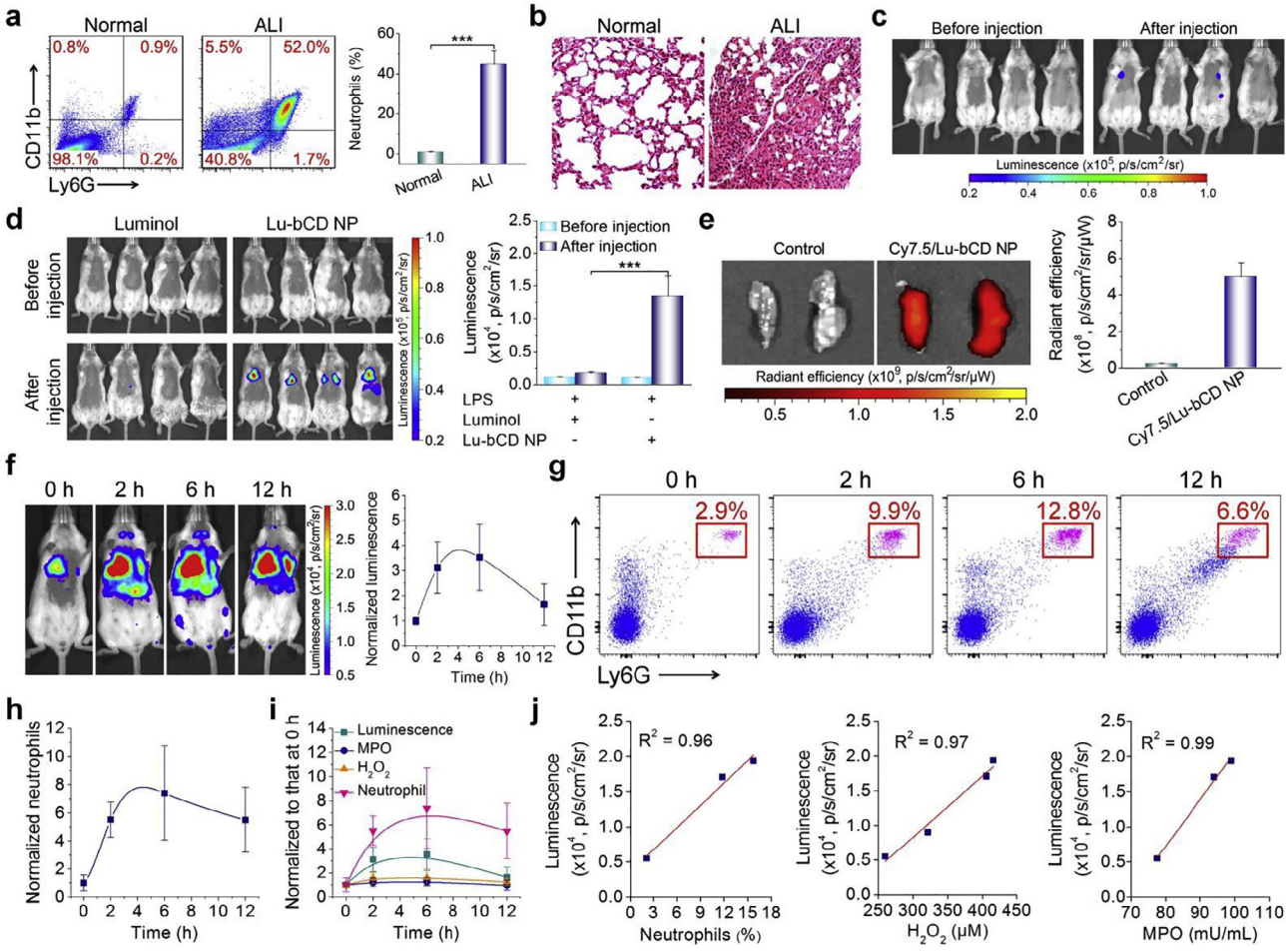

FIGURE 5

Luminescence imaging of acute lung injury (ALI) in mice induced by intratracheal (*i.t.*) inoculation of LPS. (a) Representative flow cytometric profiles (left) and quantitative analysis (right) of neutrophil counts in pulmonary tissues of ALI mice. (b) H&E stained histological sections illustrating infiltration of inflammatory cells into the lungs. (c) *In vivo* luminescence images of normal mice before and after *i.v.* injection of Lu-bCD NP. (d) Representative *in vivo* images (left) and quantitative results (right) of luminescence imaging in ALI mice before and after *i.v.* injection of luminol or Lu-bCD NP at the same dose of Lum. (e) *Ex vivo* fluorescence imaging indicates pulmonary targeting by Lu-bCD NP. (f) *In vivo* luminescence images of ALI mice at different time points after *i.v.* administration of Lu-bCD NP. The left panel shows representative images, while the right panel indicates normalized luminescence intensities. (g and h) Representative flow cytometric profiles (g) and quantitative analysis (h) showing neutrophil counts in pulmonary tissues isolated from mice at defined time points after *i.t.* inoculation of LPS. (i) The relative levels of luminescent intensities, neutrophil counts, MPO, and H_2O_2 in the lungs from mice at defined time points after *i.t.* inoculation of LPS. (j) Correlation analysis of luminescent intensities with the neutrophil count as well as the level of H_2O_2 or MPO. Error bars, mean þ s.d. ($n = 6$, a, h–i; $n = 4$, d–f); $^{*}P < 0.05$, $^{**}P < 0.01$, $^{***}P < 0.001$.

Safety studies

Finally, *in vitro* and *in vivo* evaluations were conducted to test the safety of Lu-bCD NP applications. In both normal and tumor cell lines, even 500 lg ml^{-1} of Lu-bCD NP did not cause noticeable cytotoxicity (Fig. S10). Since previous studies indicated that platelets may be activated by some nanomaterials [37–39], possible effects of Lu-bCD NP treatment on platelets were examined. Treatment of whole blood with various doses of Lu-bCD NP did not induce notable platelet aggregation (Fig. S11a-b). Quantification of representative blood coagulation parameters, including the plasma level of fibrinogen (FBG), prothrombin time (PT), thrombin time (TT), and activated partial thromboplastin time (APTT), revealed no significant changes after incubation of platelets with varied concentrations of Lu-bCD NP (Fig. S11c-f). Consistently, immunofluorescence analysis suggested that platelets were not activated by Lu-bCD NP (Fig. S11g). It should be emphasized that 30 mg ml^{-1} of Lu-bCD NP is dramatically higher than its plasma level after *i.v.* administration for *in vivo* imaging in ALI mice.

After a single *i.v.* injection at 600 mg kg^{-1} in model mice, no significant changes in the body weight and organ index of major organs were observed (Fig. S12a-b). Complete blood count revealed no abnormal variations in the number of red blood cells, white blood cells, and platelets as well as the level of hemoglobin (Fig. S12c). Clinical biochemistry analysis did not find abnormal changes for biomarkers related to hepatic and kidney functions (Fig. S12d). Analysis on H&E stained sections also showed no histological abnormity appeared in major organs (Fig. S12e). Together, these data demonstrated Lu-bCD NP is safe for *in vivo* applications at the examined dose that is at least sixfold higher than those required for *in vivo* imaging by *i.v.* administration. This is consistent with *in vitro* results that

Lu-bCD NP can be completely hydrolyzed into biocompatible small molecules, and the resulting metabolites are then more readily excreted. It is also in line with the fact that b-CD and its derivatives have been broadly employed in pharmaceutical formulations administered via different routes [32,40,41], and luminol itself has been used as a drug for the treatment of alopecia areata [42].

Conclusion

In summary, we have developed a luminescent nanoplatform by facile self-assembly of a b-CD-derived amphiphile, with amplified and sustained luminescence. Activated neutrophils were selectively imaged using this nanoprobe. Responding to neutrophil counts as well as abnormal levels of ROS and MPO, this newly engineered nanoprobe showed desirable luminescence for the detection of different inflammatory disorders in both superficial and deep tissues, enabling noninvasive and real-time detection of initiation, progression, and resolution of inflammation. This strategy can also provide important information for high-throughput and high-content screening of anti-inflammatory therapeutics. In addition, this nanoplatform can be used as a MPO-triggerable nanovehicle for site-specific delivery of a large number of therapeutic or contrast agents for combination therapy or multimodality molecular imaging.

Acknowledgements

This study was supported by the National Natural Science Foundation of China (No. 81471774), the Research Foundation of Third Military Medical University (No. 2014XJY04), and the Graduate Student Research Innovation Project of Chongqing.

Appendix A. Supplementary data

Supplementary data associated with this article can be found, in the online version, at http://dx.doi.org/10.1016/j.mattod.2017.09.003.

References

[1] F.L. Heppner et al., Nat. Rev. Neurosci. 16 (2015) 358–372.
[2] F.K. Swirski, M. Nahrendorf, Science 339 (2013) 161–166.
[3] E. Elinav et al., Nat. Rev. Cancer 13 (2013) 759–771.
[4] G.S. Hotamisligil, Nature 444 (2006) 860–867.
[5] D.C. Dale et al., Blood 112 (2008) 935–945.
[6] O. Soehnlein et al., Trends Immunol. 30 (2009) 538–546.
[7] A. Mantovani et al., Nat. Rev. Immunol. 11 (2011) 519–531.
[8] E. Kolaczkowska, P. Kubes, Nat. Rev. Immunol. 13 (2013) 159–175.
[9] K. Hoenderdos, A. Condliffe, Am. J. Respir. Cell Mol. Biol. 48 (2013) 531–539.
[10] H.L. Wright et al., Nat. Rev. Rheumatol. 10 (2014) 593–601.
[11] B.M. Fournier, C.A. Parkos, Mucosal Immunol. 5 (2012) 354–366.
[12] C. Weber et al., Nat. Rev. Immunol. 8 (2008) 802–815.
[13] C.T. Murphy et al., Clin. Exp. Immunol. 162 (2010) 188–196.
[14] M. Edinger et al., Methods 31 (2003) 172–179.
[15] L.R. DeChatelet et al., J. Immunol. 129 (1982) 1589–1593.
[16] M.K. So et al., Nat. Biotechnol. 24 (2006) 339–343.
[17] S. Gross et al., Nat. Med. 15 (2009) 455–461.
[18] N. Zhang et al., Nat. Med. 19 (2013) 500–505.
[19] W.T. Chen et al., Mol. Imaging 3 (2004) 159–162.
[20] A. Kielland et al., Free Radic. Biol. Med. 47 (2009) 760–766.
[21] B.S. van der Veen et al., Antioxid. Redox Signal. 11 (2009) 2899–2937.
[22] J.M. Sanders et al., Xenobiotica 30 (2000) 263–272.
[23] Y. Li et al., Adv. Mater. 27 (2015) 4075–4080.
[24] A.J. Shuhendler et al., Nat. Biotechnol. 32 (2014) 373–380.
[25] S.L. Gai et al., Chem. Rev. 114 (2014) 2343–2389.
[26] L. Tong, J.X. Cheng, Mater. Today 14 (2011) 264–273.
[27] J.H. Park et al., Nat. Mater. 8 (2009) 331–336.
[28] D. Lee et al., Nat. Mater. 6 (2007) 765–769.
[29] S.R. Sturzenbaum et al., Nat. Nanotechnol. 8 (2013) 57–60.
[30] Z. Hu et al., Chem. Soc. Rev. 43 (2014) 5815–5840.
[31] P.M. Fauchet, Mater. Today 8 (2005) 26–33.
[32] M.E. Davis, M.E. Brewster, Nat. Rev. Drug Discov. 3 (2004) 1023–1035.
[33] W.M. Nauseef, Cell. Microbiol. 16 (2014) 1146–1155.
[34] C.J. Morris, Methods Mol. Biol. 225 (2003) 115–121.
[35] Q.X. Zhang et al., Biomaterials 105 (2016) 206–221.
[36] G. Matute-Bello et al., Am. J. Physiol. Lung Cell. Mol. Physiol. 295 (2008) L379–399.
[37] S. Deb et al., Nanomedicine. NBM 7 (2011) 376–384.
[38] S. Deb et al., Nanotoxicology 1 (2006) 93–103.
[39] J. Cheng et al., ACS Nano 10 (2016) 9957–9973.
[40] J.X. Zhang, P.X. Ma, Adv. Drug Deliv. Rev. 65 (2013) 1215–1233.
[41] J.X. Zhang, P.X. Ma, Nano Today 5 (2010) 337–350.
[42] S. Irie, Curr. Ther. Res. Clin. Exp. 2 (1960) 107–110.